

First principles study on geometric and electronic properties of two-dimensional Nb_2CT_x MXenes

Guoliang Xu(徐国亮), Jing Wang(王晶), Xilin Zhang(张喜林), and Zongxian Yang(杨宗献)

Citation: Chin. Phys. B, 2022, 31 (**3**): 037304. DOI: 10.1088/1674-1056/ac322e
Journal homepage: http://cpb.iphy.ac.cn; http://iopscience.iop.org/cpb

What follows is a list of articles you may be interested in

Signatures of strong interlayer coupling in γ-InSe revealed by local differential conductivity

Xiaoshuai Fu(富晓帅), Li Liu(刘丽), Li Zhang(张力), Qilong Wu(吴奇龙), Yu Xia(夏雨), Lijie Zhang(张利杰), Yuan Tian(田园), Long-Jing Yin(殷隆晶), and Zhihui Qin(秦志辉)

Chin. Phys. B, 2021, 30 (**8**): 087306. DOI: 10.1088/1674-1056/abff32

Collective excitations and quantum size effects on the surfaces of Pb(111) films: An experimental study

Yade Wang(王亚德), Zijian Lin(林子荐), Siwei Xue(薛思玮), Jiade Li(李佳德), Yi Li(李毅), Xuetao Zhu(朱学涛), and Jiandong Guo(郭建东)

Chin. Phys. B, 2021, 30 (**7**): 077308. DOI: 10.1088/1674-1056/abfbcd

Seeing Dirac electrons and heavy fermions in new boron nitride monolayers

Yu-Jiao Kang(康玉娇), Yuan-Ping Chen(陈元平), Jia-Ren Yuan(袁加仁), Xiao-Hong Yan(颜晓红), Yue-E Xie(谢月娥)

Chin. Phys. B, 2020, 29 (**5**): 057303. DOI: 10.1088/1674-1056/ab7e9e

General principles to high-throughput constructing two-dimensional carbon allotropes

Qing Xie(谢庆), Lei Wang(王磊), Jiangxu Li(李江旭), Ronghan Li(李荣汉), Xing-Qiu Chen(陈星秋)

Chin. Phys. B, 2020, 29 (**3**): 037306. DOI: 10.1088/1674-1056/ab6c4b

Enhanced performance of a solar cell based on a layer-by-layer self-assembled luminescence down-shifting layer of core-shell quantum dots

Ni Liu(刘妮), Shu-Xin Li(李淑鑫), Ying-Chun Ye(叶迎春), Yan-Li Yao(姚延立)

Chin. Phys. B, 2018, 27 (**12**): 127303. DOI: 10.1088/1674-1056/27/12/127303

First principles study on geometric and electronic properties of two-dimensional Nb_2CT_x MXenes

Guoliang Xu(徐国亮), Jing Wang(王晶), Xilin Zhang(张喜林)[†], and Zongxian Yang(杨宗献)[‡]

Henan Key Laboratory of Photovoltaic Materials, School of Physics, Henan Normal University, Xinxiang 453000, *China*

(Received 9 August 2021; revised manuscript received 28 September 2021; accepted manuscript online 22 October 2021)

MXenes are a new type of two-dimensional carbides with rich physical and chemical properties. The physics of MXenes, and thus the applications, are dominated by surface functional groups. Herein, the effects of different terminations (O, S, Se, Te) on the geometric and electronic properties of Nb_2C MXenes were studied *via* density functional theory (DFT) calculations. Three adsorption sites were examined to determine the most stable configurations. The results showed that both the types and the positions of surface functional groups influence the geometric stability and physical characters of Nb_2C. The S and Se terminations make the Nb_2C MXenes to be semiconductor, while Nb_2C MXenes with other terminations (O, Te) are conductor. The electron location function, density of states, Bader charge distribution, and the projected crystal orbital Hamilton population were conducted to explain the origin of adsorption stability and electronic nature difference. Our results provide a fundamental understanding about the effects of surface terminations on the intrinsic stability and electronic properties of Nb_2C MXenes.

Keywords: Nb_2C MXenes, surface functional groups, geometric structure, electronic properties

PACS: 73.20.At, 73.22.–f, 63.20.dk, 31.15.es **DOI:** 10.1088/1674-1056/ac322e

1. Introduction

Two-dimensional (2D) materials such as graphene,[1,2] transition metal dichalcogenides,[3] phosphorene,[4] *etc.* have attracted intensive attention and were widely used in energy storage, catalysis, and electronic devices. In recent years, a new family of 2D materials called MXenes[5–7] were routinely synthesized by selectively etching the A-layer elements from the MAX ceramic phases with diluted hydrofluoric acid. The residual 2D MX layers are often covered by surface groups like O, OH, or F, giving a general formula of $M_{n+1}X_nT_x$, where M is an early transition metal, X is carbon and/or nitrogen, and T_x represents surface terminations on the metal layers. Since the first $Ti_3C_2T_x$ MXenes was reported,[5] a large number of MXenes have emerged and shown promising applications in energy storage,[8,9] sensors,[10,11] electromagnetic interference shielding,[12] catalysis,[13] *etc.*, owing to the charming physiochemical properties. Especially, the intrinsic nature of MXenes vary with elements at the metal site, C/N site, as well as the surface terminations.

For a specific MXenes, surface groups influence the electronic properties and the potential applications because of different electronegativity and stable sites. For instance, the majority-spin and minority-spin electrons of bare Cr_2C respectively have metal and insulator properties, giving a half-metallic ferromagnetic Cr_2C, while Cr_2CF_2 and $Cr_2C(OH)_2$ are antiferromagnetic, because the majority-spin dispersions hold the same characters as the minority-spin electrons.[14] The band dispersions of bare Sc_2C showed that the Fermi level is occupied by the Sc-d band, leading to a metallic Sc_2C. When it is terminated with F/OH, the Fermi level of Sc_2C moves to the center of the energy gap, and Sc_2CF_2 and $Sc_2C(OH)_2$ become semiconductors. Because O atom needs more electrons than F/OH, and Sc atoms alone cannot provide enough electrons to oxygen group, so parts of O atoms prefer to be adsorbed at the top of C, giving an insulating Sc_2CO_2.[15]

The above findings demonstrate that both the type and position of functional groups on MXenes surface have a deep influence on the electronic structure of MXenes, and thus the potential applications. Kan *et al.*[16] used Nb_2CT_2 (T = O/F/OH) MXenes as substrate of Pt/Pd atoms to explore the modification effect of surface functional groups on the stability and activity by density functional theory. Their results showed that the O/F termination has a good fixation effect toward doped Pt/Pd atoms in comparison with the OH groups. In addition, the O/F functional groups can optimize the electronic structure of Pt/Pd atoms, leading to moderate adsorption of oxygenates. Recently, the Nb-based MXenes covered with S, Se, and Te groups were synthesized by combinations of etching and substitution reactions using Lewis acidic/basic molten salts.[17] The etching of Ti_3AlC_2 MAX phase in molten $ZnCl_2$ and several other Lewis acidic molten salts above 500 °C results in the $Ti_3C_2Cl_2$ MXenes with a pure Cl termination. Similar methods also were used to synthesize other MXenes including Nb_2CCl_2. Compared with the F/OH functional groups, the halogen functional groups are more likely to participate in a new type of surface ex-

[†]Corresponding author. E-mail: zhangxilin@htu.edu.cn
[‡]Corresponding author. E-mail: yzx@htu.edu.cn

© 2022 Chinese Physical Society and IOP Publishing Ltd

change reaction to generate S/Se/Te terminated MXenes, due to the weak surface bonding interaction.[17] These MXenes exhibit unique structural and electronic properties, such as a large in-plane lattice expansion and superconductivity. Moreover, Nb_2CSe_2 powder samples were synthesized by the traditional high temperature solid-state synthesis method.[18] The prepared Nb_2CSe_2 samples demonstrated good conductivity, abundant active sites, low cost, and high oxygen evolution activity, because the resultant TMD-MXenes like structures simultaneously have electro-conductive Nb–C layer and rich active marginal Se layer sites.

Although the Nb_2C MXenes with different terminations were prepared and investigated for various applications, a fundamental understanding on the effects of surface groups is insufficient. A comparative study on the influence of different functional groups on the geometric configuration, structural stability, electronic nature, *etc.*, is of significance for the further rational design. In this work, the geometries of four functional groups (O, S, Se, and Te) on Nb_2C were investigated based on density functional theory. It is found that the most stable sites vary with the functional groups, giving rise to different lattice parameters and orbital hybridization. From the density of states (DOS) and band diagrams, we found that the conductivity of Nb_2CT_x is affected by both the terminations and their adsorption sites. The electron localization function (ELF) results revealed that the adsorption site of T_x regulate the charger redistribution, changing the interaction strength between T_x atoms and the Nb_2C. The bonding strength of Nb–T_x was analyzed by projected crystal orbital Hamilton population (pCOHP). The results showed that the Nb–T_x bonding strength is weakened with the decrease of electronegativity of functional groups (O > S > Se > Te), contributing to the feasible formation of the surface vacancy.

2. Computational methods

The spin-unrestricted calculations were performed within the framework of density functional theory (DFT) using the Vienna *ab initio* simulation package (VASP).[19] A plane wave cut off energy of 500 eV was used for the plane-wave expansion of the wave function. The potentials at the core region were treated with projector augmented wave (PAW) pseudopotentials.[20] The exchange–correlation energy was represented by a gradient corrected,[20,21] functional proposed by Perdew, Burke, and Ernzerhof (PBE).[22] Brillouin zone integrations were performed using a $9 \times 9 \times 1$ Monkhorst–Pack[23] K-point mesh for geometry optimizations, and the convergence threshold was set to be 10^{-6} eV in energy and 0.01 eV/Å in force. The convergence of geometrical parameters was also tested. For density of states calculations the Brillouin zone was sampled using a $13 \times 13 \times 1$ K-grids. In all the structures, vacuum regions between two adjacent periodic images were over 16 Å to avoid spurious interaction between periodic images. After examining the effects of Hubbard U and van der Waals corrections on the geometric parameters of Nb_2C (Table S1) and comparing with previous results, we just consider the van der Waals corrections under D3 scheme.[24] The determination of the bonding and antibonding states between M and T_x atoms was obtained by the projected crystal orbital Hamilton population (pCOHP)[25–28] as employed by the Lobster program. COHP is a partitioning of the band-structure energy in terms of orbital-pair contributions and it is abond-weighted density-of-states between a pair of adjacent atoms. Deringer and coworkers further developed the projected COHP (pCOHP) by re-extracting Hamilton-weighted populations from plane-wave electronic-structure calculations.[26] The IpCOHP stands for the integral value below the Fermi level of pCOHP, it can be understood as the number of bonded electrons shared between two atoms.

3. Results and discussion

We focused on the geometric configurations and electronic properties of monolayer Nb_2C and Nb_2CT_x (T_x = O, S, Se, and Te). The Nb_2C monolayer is composed of three atomic layers stacked in a sequence of Nb(A)–C–Nb(B) (Figs. 1(a) and 1(b)). Three possible configurations of terminations are considered: type I (Fig. 1(c)), the surface groups are located directly above the top site of C atoms; type II (Fig. 1(d)), the groups that are connected to the Nb(A) atoms are at the top sites of the central C atoms and the others are at the hollow sites of Nb(B) atoms, forming an asymmetric arrangement on the Nb_2C layer; type III (Fig. 1(e)), the groups are located at the central C hollow sites on both sides of Nb_2C layer. In the following section, we will use the nomenclature defined in Fig. 1 for simplification. The optimized Nb_2C has an in-plane lattice constant of 3.107 Å accompanied with the Nb–C bond length of 2.15 Å, agreeing with the experimental[29,30] and theoretical

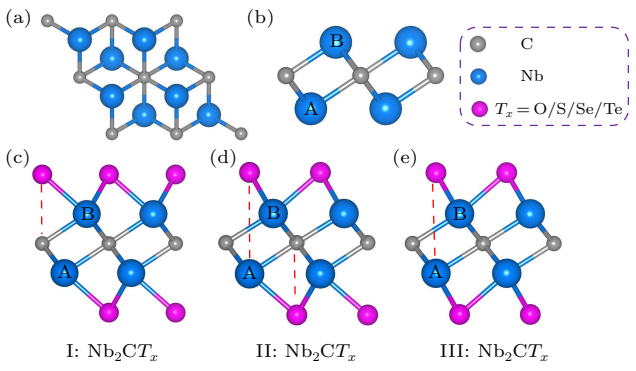


Fig. 1. The structure of Nb_2C and Nb_2CT_x (T_x = O, S, Se, and Te). Top view (a) and side view (b) of 2D Nb_2C. Side view of three probable Nb_2CT_x configurations.

reports.[31,32] The total energies of all the MXenes with different termination groups are shown in Table S2 of the supporting information. Upon terminated with O and Te functional groups, configuration III become the most stable structure due to the lowest total energy relative to the other configurations, while the most stable structure is configuration II for the S and Se groups. The phonon dispersions are shown in Fig. S1 to verify the dynamic stabilities. The positive phonon frequencies indicate the dynamic stabilities of III-Nb_2CO_2, II-Nb_2CS_2, and II-Nb_2CSe_2. The III-Nb_2CTe_2 is dynamically unstable due to the existence of imaginary frequencies. The geometric parameters of Nb_2CT_x (T_x = O, S, Se, and Te) are summarized in Table 1 for comparatively understanding the influences of functional groups on the structure of MXenes. For the O/S/Se groups, the lattice constant of MXenes gradually increases from configurations I–III as the surface groups migrate. For Te-terminal MXenes, the configuration II has the largest lattice constant. For the same configuration of Nb_2CT_x MXenes, as the electronegativity of the functional group gradually decreases from O through S and Se to Te, the lattice constant of MXenes and the Nb–T_x bond lengths gradually increase, while the T_x–Nb–T_x angle gradually decreases from O to Te, reflecting the different chemical bond strength between the functional groups and Nb atoms.

Table 1. The geometric parameters of Nb_2CT_x (T_x = O, S, Se, and Te) at three configurations. The superscripts a and b mean the bond length of Nb(B)–T_x and Nb(A)–T_x.

	Lattice constant (Å)			Nb–T_x bond length (Å)			T_x–Nb–T_x angle (°)		
	I	II	III	I	II	III	I	II	III
Nb_2CO_2	3.035	3.080	3.125	2.100	2.094^a 2.115^b	2.090	92.251	94.773	96.646
Nb_2CS_2	3.210	3.250	3.258	2.489	2.489^a 2.490^b	2.498	80.301	81.488	81.389
Nb_2CSe_2	3.274	3.299	3.301	2.618	2.620^a 2.619^b	2.628	77.463	78.115	77.751
Nb_2CTe_2	3.369	3.390	3.385	2.818	2.813^a 2.815^b	2.835	73.443	74.100	73.458

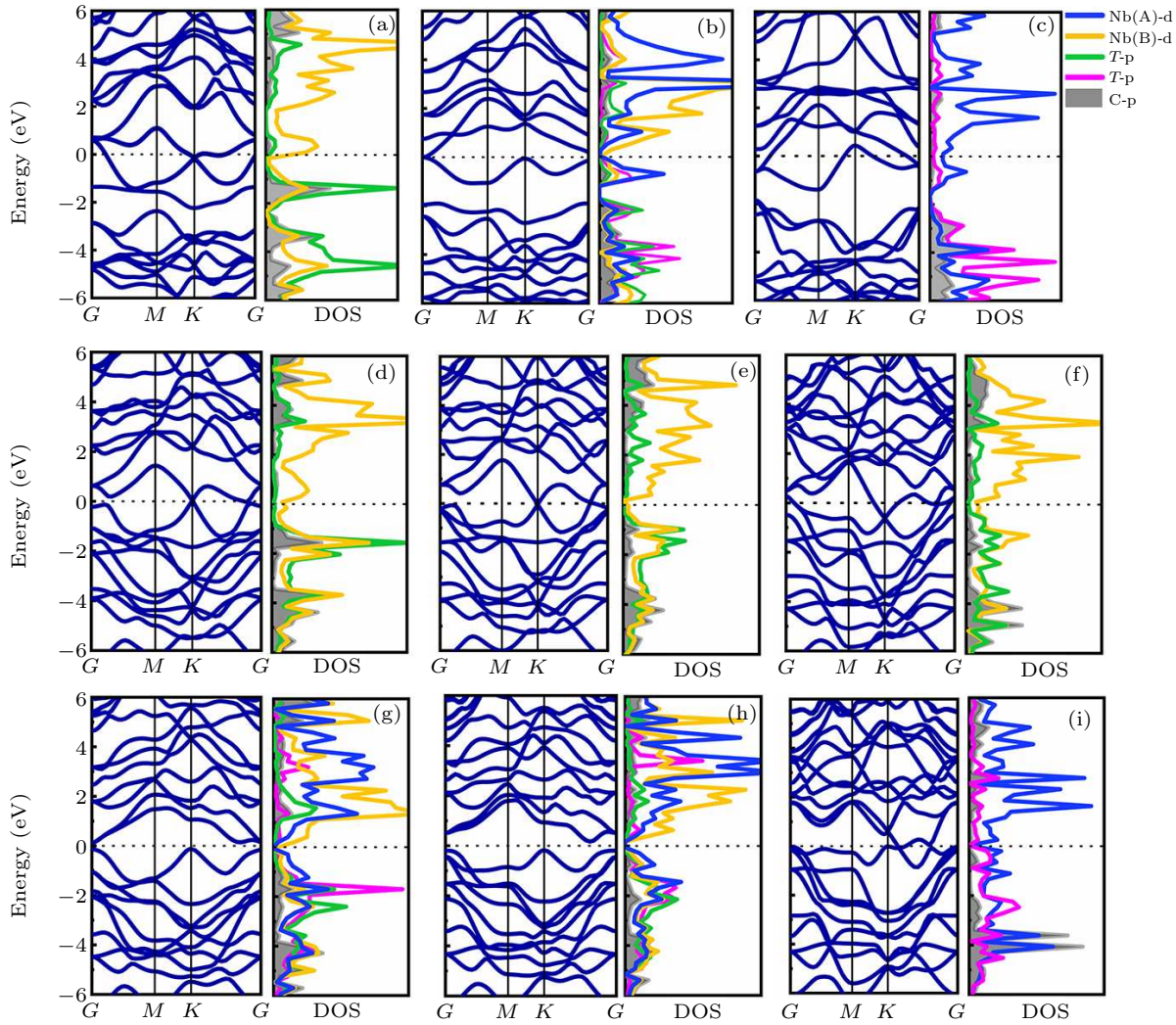


Fig. 2. Band dispersions and density of states (DOS) of the Nb_2CT_x monolayer. (a) I-Nb_2CO_2; (b) II-Nb_2CO_2; (c) III-Nb_2CO_2; (d) I-Nb_2CS_2; (e) I-Nb_2CSe_2; (f) I-Nb_2CTe_2; (g) II-Nb_2CS_2; (h) II-Nb_2CSe_2; and (i) III-Nb_2CTe_2.

The Nb_2C MXenes is conductor, since the 4d states of Nb atoms pass through the Fermi level (Fig. S2). The electronic properties of Nb_2CT_x layer are strongly related to the functional groups on the surface. When the surface is terminated by O atoms, all the three configurations (Figs. 2(a)–2(c)) show metallicity. Interestingly, when terminated with S and Se, the resultant MXenes monolayer can be narrow-band gap semiconductors or metals, depending on the arrangement modes. The most stable II-Nb_2CS_2 (Fig. 2(g) and S3(b)) exhibits a semiconducting character with an energy gap of 0.32 eV under the scheme of Heyd–Scuseria–Ernzerhof (HSE06) hybrid functional.[33] The projected DOS analyses show that the conduction band minimum and the valance band maximum are contributed by the d states of Nb(B) and Nb(A) atoms, respectively. The I-Nb_2CS_2 (Fig. 2(d)) and III-Nb_2CS_2 (Fig. S4(c)) are however metallic. Similar to Nb_2CS_2 monolayer, the most favorable II-Nb_2CSe_2 (Fig. 2(h)) has a semiconductor characteristic, while both I-Nb_2CSe_2 (Fig. 2(e)) and III-Nb_2CSe_2 (Fig. S4(f)) are metallic with limited electronic states crossing the Fermi level. When the surface is terminated by Te, the Nb_2CTe_2 (Figs. 2(f), 2(i), and S4(h)) show metal characteristics like Nb_2CO_2. The above findings indicate that the band structures of MXene are affected by both the types and positions of groups, which are determined by the bonding characters and the orbital hybridization. So the projected densities of states (PDOS) are analyzed to further clarify the contribution of different atoms.

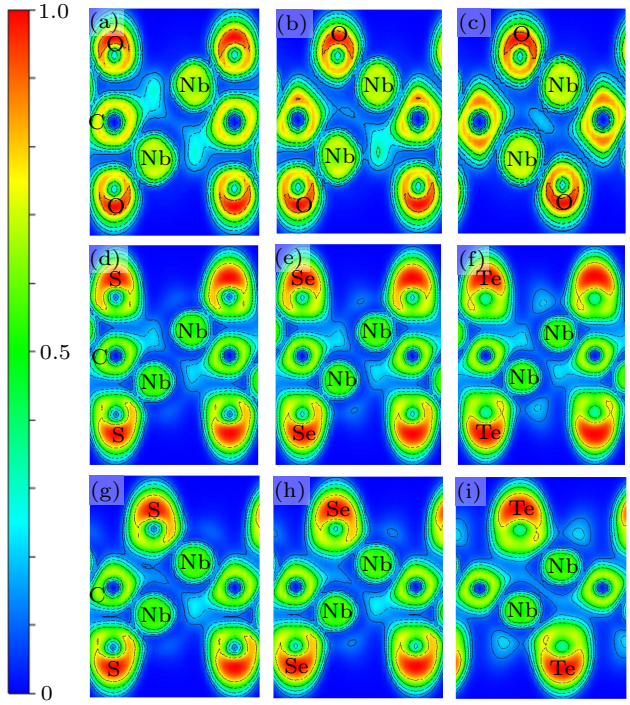


Fig. 3. The 2D slices projected along direction of electron localization function (ELF) are plotted. Upper panel shows the ELF plots for (a) I-Nb_2CO_2, (b) II-Nb_2CO_2, (c) III-Nb_2CO_2, middle panel shows the ELF for (d) I-Nb_2CS_2, (e) I-Nb_2CSe_2, (f) I-Nb_2CTe_2; and lower panel shows (g) II-Nb_2CS_2, (h) II-Nb_2CSe_2, and (i) III-Nb_2CTe_2.

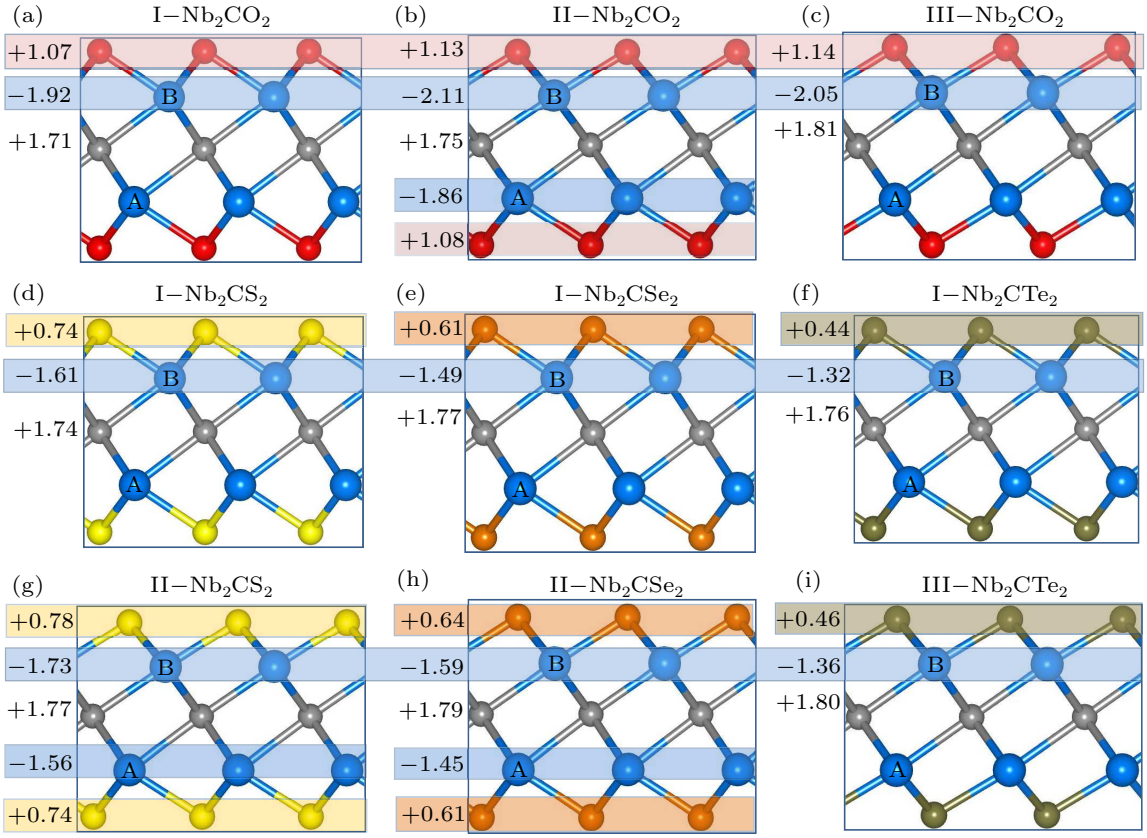


Fig. 4. Bader charge analysis revealing the relative charge transfer between various atoms during the structural phase formation of (a) I-Nb_2CO_2, (b) II-Nb_2CO_2, (c) III-Nb_2CO_2; middle panel shows (d) I-Nb_2CS_2, (e) I-Nb_2CSe_2, (f) I-Nb_2CTe_2; and lower panel shows (g) II-Nb_2CS_2, (h) II-Nb_2CSe_2, and (i) III-Nb_2CTe_2. Plus symbol "+" indicates the gain of electrons and minus symbol "−" indicates the loss of electrons.

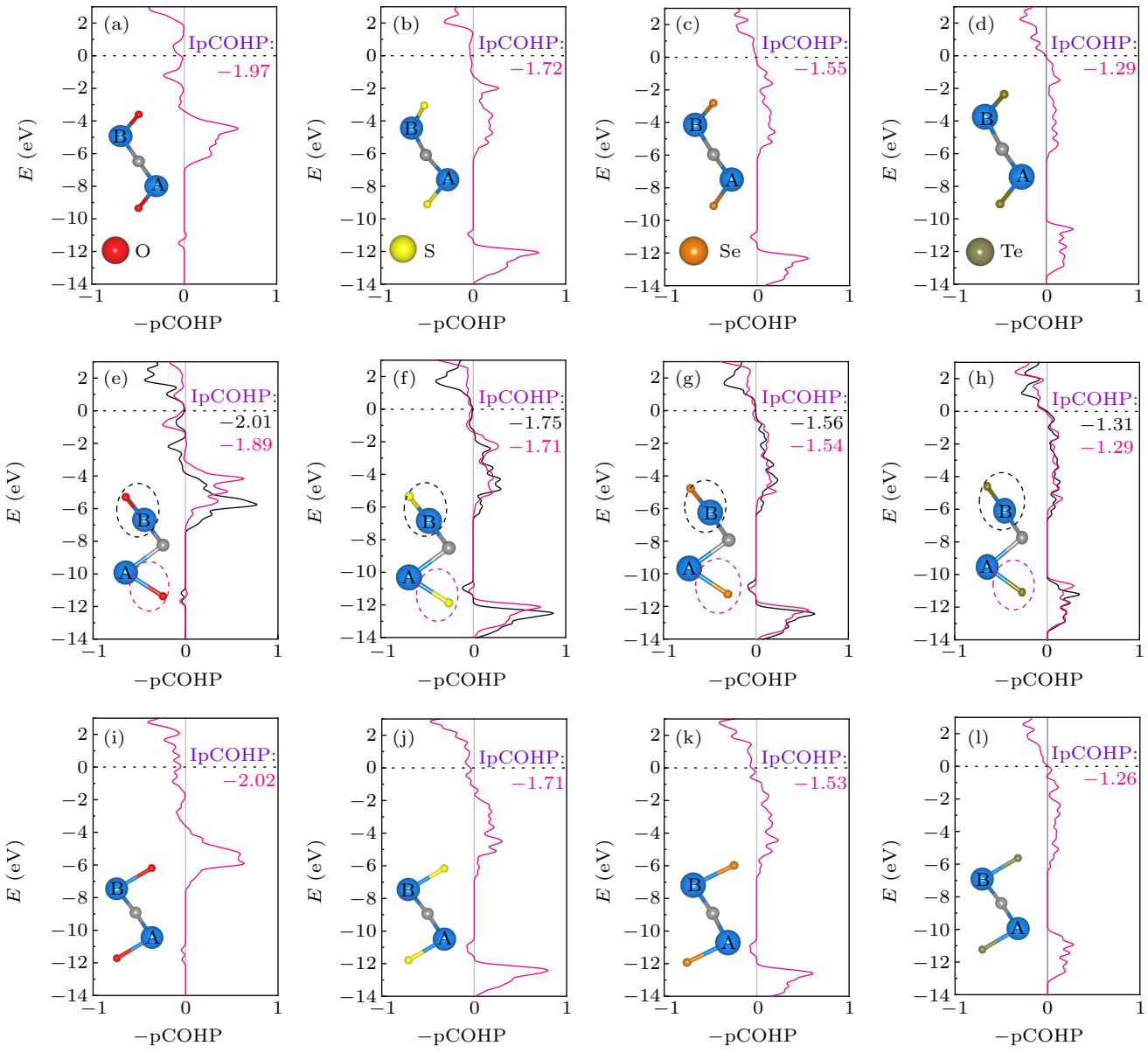


Fig. 5. The projected crystal orbital Hamilton population (pCOHP) states have been plotted for the Nb_2CT_x. (a)–(d) I-Nb_2CT_x (in which T_x represents O, S, Se, and Te); (e)–(h) II-Nb_2CT_x (in which T_x represents O, S, Se, and Te); (i)–(l) III-Nb_2CT_x (in which T_x represents O, S, Se, and Te).

As shown in Fig. 2(a), at the configuration I, the weak interactions among Nb, O, and C atoms are supported by the negligible overlap between Nb-d states with O/C-p states. For the configuration II (Fig. 2(b)), a strong overlap between Nb(B)-d and C/O-p in the energy range of −1 eV to 0 eV and −4.5 eV to −3 eV makes the structure more stable. In configuration III (Fig. 2(c)), an even strong overlap between Nb-d and O/C-p can be observed from −6 eV to Fermi level, indicating a strong bonding interaction between these atoms. Different from Nb_2CO_2, the configuration II of Nb_2CS_2 has a strong hybridization between Nb(B)-d and C/S-p in the energy range of −3.5 eV to −1 eV and −6 eV to −4.5 eV, making it stable. The similar phenomena are observed on the Nb_2CSe_2 and Nb_2CTe_2.

In order to further study the effect of surface functional groups on the structural stability, we performed an electron localization function (ELF) analysis (Fig. 3). The value of ELF between two atoms can be in the range of 0 to 1, where 1, 0.5, and 0 represent covalent, metallic, and no-bonding characters, respectively.[34,35] Taking Nb_2CO_2 as examples, a weak electron-gas between Nb and C together with a highly concentrated electrons around C are observed, showing the metallic–ionic character of the Nb–C bonds. This conclusion is applicable to Nb–O bonds. For configuration II (Fig. 3(b)), when one O atom is migrated to the hollow site, an increased localized electron around O enhances the ionic bond between Nb and O, and this is conducive to the improved stability. In configuration III (Fig. 3(c)), when all O groups locate at the hollow sites, the electrons localized around C and O increase obviously, which makes it more stable. These results may explain why the O groups prefer to the hollow site.

When the S atom is placed at the hollow site of Nb(A)

atoms (configuration II and Fig. 3(g)), the localized electrons among Nb, C, and S are larger than the configuration I and configuration III (Figs. 3(d) and S6(c)), demonstrating the strong bonding interaction and structural stability. Nb_2CSe_2 has similar bonding characters to Nb_2CS_2, as shown in Figs. 3(e) and 3(h). The ionic characters of Nb–C and Nb–Se can be concluded from the large ELF value of near the C and Se atoms in configuration II. In addition, in configuration III of Nb_2CTe_2, Nb atoms form a strong ionic bond with the surface Te atoms.

We further performed the Bader charge analyses in Fig. 4 to quantitatively estimate the adsorption strength of surface groups on Nb_2C surface. It is found that the charge is always transferred from Nb to C and surface groups. In comparison with configurations I and II, the O and C atoms in configuration III gain more electrons, therefore enhancing the bonding interaction between Nb and O/C atoms. It also explains why the O atoms tend to adsorb at the hollow sites. From Figs. 4(d) and 4(g), the Nb_2CS_2 in configuration II can transfer more electrons from Nb(B) atom to C and S atoms, while the electron transfer from Nb(A) is fewer, in comparison with that in configuration I. The similar situation is found for the surface terminated by Se and Te functional groups.

To further assess the bond strength of Nb_2CT_x MXenes, the projected crystal orbital Hamilton population (pCOHP) calculations were carried out. Figure 5 shows the integrated pCOHP dispersions and the corresponding integration values, which are efficient measure of the bonding strength. Compared with the Nb–C bonding contribution, Nb–T_x bonding is a dominant factor for surface bonding strength. With the decrease of electronegativity of functional groups, the bonding strength of Nb–T_x gradually decreases for the same configuration. The structure with a weak Nb–T_x chemical bond strength is easier to form surface vacancy. Obviously, compared with other structures, the IpCOHP value of Nb–Te in configuration III (Fig. 5(l)) is the smallest, demonstrating the weakest bonding interaction and the easiest formation of surface vacancy, in line with the experimental element analyses.[18] For configuration II, the distinct adsorption sites for surface groups lead to imbalanced interaction strength associated with different IpCOHP value (Figs. 5(e)–5(h)), the bond strength of Nb(B)–T_x is generally stronger than that of Nb(A)–T_x.

4. Conclusion

In conclusion, based on density functional theory calculations, we systematically studied the structural stability and electronic properties of the 2D Nb_2CT_x (T_x = O, S, Se, and Te), with particular attention on the effects of surface groups. It is found that the O and Te groups prefer to the central C hollow sites on both sides of Nb_2C, while the most stable sites for the S and Se terminations are unequable on the two Nb_2C sides. The interaction strength between Nb atoms and functional groups decrease gradually from O through S and Se to Te. The bonding interaction was analyzed by the electron location function, Bader charge, and the projected crystal orbital Hamilton population. From O to Te groups, the surface terminations gain fewer electrons, and the integrated pCOHP value gradually reduced. The changed interaction will modify the electronic nature of Nb_2C MXenes. The types of surface groups dominate the electronic characters and conductivity, and the adsorption sites are the secondary influencing factor. The Nb_2CO_2 and Nb_2CTe_2 always have metallicity. The Nb_2CS_2 and Nb_2CSe_2 can be semiconductor or metal, depending strongly on the adsorption sites of surface groups on Nb_2C. We anticipate that the present results could provide some insights into the fundamental understanding toward the effects of surface groups to the MXenes.

Acknowledgments

Project supported by the National Natural Science Foundation of China (Grant Nos. U1804130, U2004212, 11904084, and 11874141), the Henan Overseas Expertise Introduction Center for Discipline Innovation (Grant No. CXJD2019005), the China Postdoctoral Science Foundation (Grant No. 2021M690933), and the Key Scientific Research Projects of Henan Education Department, China (Grant No. 22A140020). The simulations are performed on resources provided by the High Performance Computing Center of Henan Normal University.

References

[1] Yoo E and Zhou H 2011 *ACS Nano* **5** 3020
[2] Shen J, Zhu Y, Yang X and Li C 2012 *Chem. Commun.* **48** 3686
[3] Song X, Guo Z, Zhang Q, Peng Z and Zhang D W 2017 *Small* **13** 1700098
[4] Zhang J L, Han C, Hu Z, Wang L, Liu L, Wee A T S and Chen W 2018 *Adv. Mater.* **30** 1802207
[5] Naguib M, Kurtoglu M, Presser V, Lu J, Niu J, Min H, Hultman L, Gogotsi Y and Barsoum M W 2011 *Adv. Mater.* **23** 4248
[6] Naguib M, Mochalin V N, Barsoum M W and Gogotsi Y 2014 *Adv. Mater.* **26** 992
[7] Anasori B, Luhatskaya M R and Gogotsi Y 2017 *Nat. Rev. Mater.* **2** 16098
[8] Tang Q, Zhen Z and Shen P 2012 *J. Am. Chem. Soc.* **134** 16909
[9] Er D, Li J, Naguib M, Gogotsi Y and Shenoy V B 2014 *ACS Appl. Mater. Interf.* **6** 11173
[10] Xiao B, Li Y C, Yu X F and Cheng J B 2016 *Sensor Actuat. B-Chem.* **235** 103
[11] Yu X F, Li Y C, Cheng J B, Liu Z B, Li Q Z, Li W Z, Yang X and Xiao B 2015 *ACS Appl. Mater. Interf.* **7** 13707
[12] Liu J, Zhang H B, Sun R, Liu Y, Liu Z, Zhou A and Yu Z Z 2017 *Adv. Mater.* **29** 1702367
[13] Ran J, Gao G, Li F T, Ma T Y, Du A and Qiao S Z 2017 *Nat. Commun.* **8** 13907
[14] Si C, Zhou J and Sun Z 2015 *ACS Appl. Mater. Interf.* **7** 17510
[15] Khazaei M, Arai M, Sasaki T, Chung C Y, Venkataramanan N S, Estili M, Sakka Y and Kawazoe Y 2013 *Adv. Funct. Mater.* **23** 2185
[16] Kan D, Wang D, Zhang X, Lian R, Xu J, Chen G and Wei Y 2020 *J. Mater. Chem. A* **8** 3097
[17] Kamysbayev V, Filatov A S, Hu H, Rui X, Lagunas F, Wang D, Klie R F and Talapin D V 2020 *Science* **369** 979

[18] Pang X, Wu T, Gu Y, Wang D, Che X, Sun D and Huang F 2020 *Chem. Commun.* **56** 9036
[19] Blöchl P E 1994 *Phys. Rev. B* **50** 17953
[20] Kresse G and Joubert D 1999 *Phys. Rev. B* **59** 1758
[21] A G K and J F B 1996 *Comp. Mater. Sci.* **6** 15
[22] Perdew J P, Burke K and Ernzerhof M 1997 *Phys. Rev. Lett.* **78** 1396
[23] Monkhorst H J and Pack J D 1976 *Phys. Rev. B* **13** 5188
[24] Grimme S, Antony J, Ehrlich S and Krieg H 2010 *J. Chem. Phys.* **132** 154104
[25] Dronskowski R and Bloechl P E 1993 *J. Phys. Chem.* **97** 8617
[26] Deringer V L, Tchougréeff A and Dronskowski R 2011 *J. Phys. Chem. A* **115** 5461
[27] Maintz S, Deringer V L, Tchougréeff A and Dronskowski R 2016 *J. Comput. Chem.* **37** 1030
[28] Nelson R, Ertural C, George J, Deringer V L, Hautier G and Dronskowski R 2020 *J. Comput. Chem.* **41** 1931
[29] Salama I, El-Raghy T and Barsoum M W 2002 *J. Alloys. Compd.* **347** 271
[30] Zhu J, Chroneos A and Schwingenschlgl U 2015 *Phys. Status Solidi-R* **9** 726
[31] Qian X, Li Y, He X, Fan H and Yun S 2011 *J. Phys. Chem. Solids* **72** 954
[32] Wang J and Zhou Y 2004 *Phys. Rev. B* **69** 214111
[33] Krukau A V, Vydrov O A, Izmaylov A F and Scuseria G E 2006 *J. Chem. Phys.* **125** 224106
[34] Silvi B and Savin A 1994 *Nature* **371** 683
[35] Mishra A, Srivastava P, Carreras A, Tanaka I, Mizuseki H, Lee K R and Singh A K 2017 *J. Phys. Chem. C* **121** 18947